






# The Antibacterial Effect, Biocompatibility, and Osteogenesis of Vancomycin-Nanodiamond Composite Scaffold for Infected Bone Defects

Meng Chen <sup>1,2</sup>, Yang Li <sup>1,2</sup>, Wen-Xiu Hou <sup>3</sup>, Da-Yong Peng <sup>1,2</sup>, Jing-Kun Li <sup>1,2</sup>, Hao-Xuan Zhang <sup>1,2</sup>

<sup>1</sup>Department of Orthopedic Surgery, The First Affiliated Hospital of Shandong First Medical University, Jinan, Shandong Province, 250014, People's Republic of China; <sup>2</sup>Department of Orthopedic Surgery, Shandong Provincial Qianfoshan Hospital, Shandong University, Jinan, Shandong Province, 250014, People's Republic of China; <sup>3</sup>Department of Spine Surgery, Shandong University Qilu Hospital, Jinan, Shandong, 250000, People's Republic of China

Correspondence: Hao-Xuan Zhang, Department of Orthopedics, The First Affiliated Hospital of Shandong First Medical University, No. 16766, Lixia District, Jingshi Road, Jinan, Shandong Province, 250014, People's Republic of China, Tel/Fax +86531-89268540, Email hoho0605@126.com

**Purpose:** The repair and treatment of infected bone defects (IBD) is a common challenge faced by orthopedic clinics, medical materials science, and tissue engineering.

**Methods:** Based on the treatment requirements of IBD, we utilized multidisciplinary knowledge from clinical medicine, medical materials science, and tissue engineering to construct a high-efficiency vancomycin sustained-release system with nanodiamond (ND) and prepare a composite scaffold. Its effect on IBD treatment was assessed from materials, cytology, bacteriology, and zoology perspectives.

**Results:** The results demonstrated that the Van-ND-45S5 scaffold exhibited an excellent antibacterial effect, biocompatibility, and osteogenesis in vitro. Moreover, an efficient animal model of IBD was established, and a Van-ND-45S5 scaffold was implanted into the IBD. Radiographic and histological analyses and bone repair-related protein expression, confirmed that the Van-ND-45S5 scaffold had good biocompatibility and osteogenic and anti-infective activities in vivo.

**Conclusion:** Collectively, our findings support that the Van-ND-45S5 scaffold is a promising new material and approach for treating IBD with good antibacterial effects, biocompatibility, and osteogenesis.

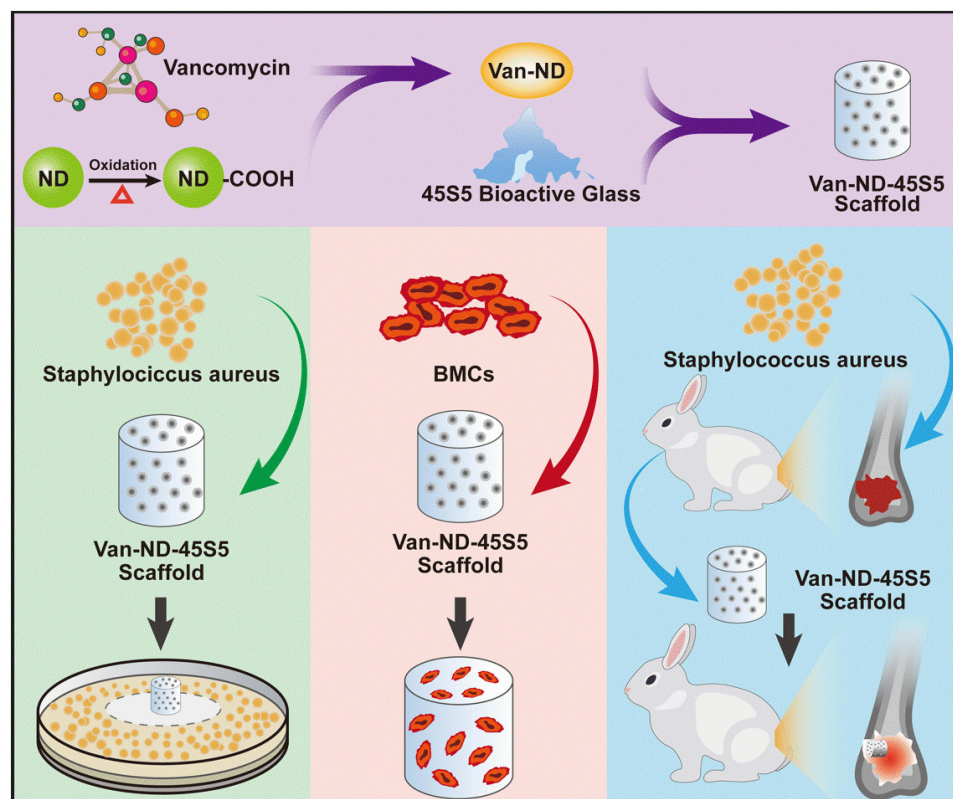
**Keywords:** antibacterial effect, nanodiamond, scaffold, infected bone defects

## Introduction

With the rapid development of mechanization and automation in agriculture, manufacturing, and transportation, the incidence of malignant accidents has also been increasing yearly. Treatment strategies for various types of open fractures and bone defects have become increasingly critical.<sup>1,2</sup> As open fractures are caused by severe high-energy trauma, foreign bodies are often left and accompanied by nerve and vascular injury, and it is difficult to achieve complete debridement at the initial stage.<sup>3,4</sup> The remaining bacteria in the infected foci gradually spread to the entire bone tissue to form acute or chronic osteomyelitis, significantly complicating subsequent treatment.<sup>5</sup> Suppurative osteomyelitis caused by delayed healing of open fractures is the most dangerous infectious bone disease in osteomyelitis, a severe complication after a fracture.<sup>6</sup> The infection focus is often located at the fracture site and gradually spreads to both ends of the bone. At a later stage, it often forms a dead cavity and causes an abscess in the surrounding soft tissue.<sup>7</sup> Abscess ruptures and forms sinus tracts, and simultaneously, osteonecrosis and nonunion repeatedly occur for a long period, eventually forming infected bone defects (IBD). IBD can cause systemic infections and endanger patients' lives, thereby increasing the difficulty of healing.<sup>8</sup>

The repair and treatment of IBD is a common challenge faced by multidisciplinary fields, such as orthopedics clinics, medical materials science, and tissue engineering.<sup>9–11</sup> Current clinical methods for repairing bone defects include bone lengthening, autologous or allogeneic bone grafting, and bone graft replacement materials, all of which have application

## Graphical Abstract



limitations.<sup>12–14</sup> Furthermore, systemic antibiotics have disadvantages, such as low concentrations of local drugs for infection, easy development of drug resistance, and systemic side effects.<sup>15,16</sup> Therefore, to control existing infections effectively and prevent possible infections, it is necessary to fill and repair bone defects using drugs that inhibit the growth and reproduction of pathogenic bacteria in the bone defect.<sup>17</sup> Composite bone graft substitute materials with osteogenic activity and local anti-infective ability to construct a local drug delivery system (DDS) can continuously provide an effective drug concentration in the infected area. Meanwhile, the blood drug concentration is low, which cannot easily cause severe systemic toxicity and side effects. The production of drug-resistant bacteria provides a practical treatment approach for IBD, attracting the attention of orthopedic physicians and scientific researchers.<sup>18,19</sup>

Vancomycin hinders cell wall synthesis by interfering with peptidoglycan, an essential component of the bacterial cell wall structure, and inhibiting the production of phospholipids and polypeptides in the cell wall to exert its bactericidal effect.<sup>20</sup> Vancomycin has a deadly impact on gram-positive bacilli and cocci that are common in IBD, such as *Staphylococcus aureus*, *Pseudomonas aeruginosa*, *Klebsiella pneumonia*, and Methicillin-resistant *Staphylococcus aureus*.<sup>21,22</sup> However, systemic application of vancomycin can easily cause toxic side effects, such as hearing loss, respiratory depression, and even liver and kidney damage.<sup>23</sup>

Although tissue engineering materials containing vancomycin have been used in the research of orthopedic diseases, their drug-loading efficiency is not ideal.<sup>24,25</sup> Previous studies have shown that compared with existing drug-carrying slow-release systems (such as polylactic-glycolic acid), surface-modified nanodiamond (ND) has a more efficient drug-carrying effect on vancomycin.<sup>26</sup> ND is an efficient sustained-release drug carrier.<sup>27,28</sup> First, the surface of ND can be designed to modify various chemical functional groups, such as hydroxyl, carbonyl, and ether, which can carry antibiotics, antitumor drugs, and growth hormones.<sup>29–31</sup> We previously functionalized ultrasonically treated ND, exposed its carboxyl functional group, and then covalently combined it with the hydroxyl functional group of vancomycin through

an ester bond to successfully prepare ND containing vancomycin.<sup>32</sup> Second, ND has stable physical and chemical properties and good biocompatibility and is exceptionally suitable as a biomedical material.<sup>33</sup> Third, the surface effect of ND result in high drug-loading efficiency, which can prolong the local residence time and improve the bioavailability of drugs.<sup>34</sup> Finally, the composite of ND and other matrix materials to prepare tissue engineered bone can significantly improve the material properties of tissue engineered bone, such as mechanical properties and wear resistance.<sup>35–37</sup>

As an ideal replacement matrix material for bone transplantation, type 45S5 bioactive glass (BG) has good biocompatibility, osteogenic activity, and degradability and promotes angiogenesis, soft tissue repair and healing.<sup>38–40</sup>

In the present study, we prepared a vancomycin-loaded ND-45S5 BG composite tissue engineering bone (Van-ND-45S5 scaffold) using bone tissue engineering technology and nanotechnology. Vancomycin is released during the local filling of IBD to inhibit common IBD pathogens and exert its osteogenic and angiogenic activities. Theoretically, it can promote the repair and healing of IBD. Through the extensive use of materials, cytology, bacteriology, and zoology, we explored the mechanism of action and prognosis of vancomycin-loaded ND-45S5 BG composite tissue engineered bone in the treatment of IBD. Our findings provide insights into the repair and treatment of IBD.

## Material and Methods

### Material

ND (NovaBone Products, LLC, USA), PLGA (50:50, MW=22,000, Medisorb, Lakeshore Biomaterials, Birmingham, AL, USA), and gelatin (Sigma-Aldrich, St. Louis, MO, USA) were used to prepare microspheres and scaffolds. The 45S5 BG powder consisted of SiO<sub>2</sub> (5 wt%), Na<sub>2</sub>O (24.5 wt%), CaO (24.5 wt%), and P<sub>2</sub>O<sub>5</sub> (6 wt%) (Aladdin Biochemical Technology Co., Shanghai, China). Vancomycin was purchased from Gold Biotechnology (St. Louis, MO, USA). *Staphylococcus aureus* ATCC25923 was acquired from the American Type Culture Collection (ATCC) (Manassas, VA, USA).

### Vancomycin-Loaded ND and Scaffold Fabrication

ND was treated with ultrasound and functionalized by an improved strong acid oxidation method,<sup>41</sup> exposing many carboxyl functional groups on its surface. It was then covalently combined with the hydroxyl functional groups of vancomycin through an ester bond to prepare the vancomycin-loaded ND. The obtained vancomycin-loaded ND and pure ND were then washed, freeze-dried for 24 h, and stored at - 20 °C. Absorbable gelatin was used as a porogen to obtain scaffolds with suitable pore sizes. The vancomycin-loaded ND and pure ND, gelatin microspheres (240 ± 32.25 µm) and 45S5 BG powder comprising a solid phase with a volume ratio of 1:1:1 were mixed with curing liquid by 3: 1 (g/mL) ratio. The mixture was sufficiently stirred to form a uniform paste and then injected into a plastic syringe (diameter, 6 mm; length, 6 mm) to obtain porous scaffolds. The fabrication process of vancomycin-loaded ND and the scaffold is presented in Figure 1.

Poly(lactic acid-glycolic acid) (PLGA) is a mature medical material widely used in medical excipients, drugs, and active cytokine sustained-release carriers.<sup>42,43</sup> Vancomycin-loaded PLGA microspheres were prepared as described previously. The same method was used to prepare vancomycin-loaded PLGA-45S5 BG composite tissue-engineered bone (Van-PLGA-45S5 scaffold) as the control group for follow-up experiments.<sup>44</sup>

All scaffolds (ND-45S5, Van-PLGA-45S5, and Van-ND-45S5 scaffolds) were lyophilized and stored at - 20 °C until further use.

### Characterization of Vancomycin-Loaded ND and Scaffold Encapsulation Efficiency

The in vitro release of vancomycin was monitored in PBS solution at 37 °C using ultraviolet-visible spectroscopy at 280 nm.<sup>45</sup> The amount of vancomycin loaded and released was determined using a standard calibration curve with known amounts of vancomycin. Moreover, the improved solid-in-oil-in-water (S/O/W) emulsification method was used to prepare vancomycin-loaded PLGA microspheres as a control group to evaluate encapsulation efficiency.<sup>44</sup>

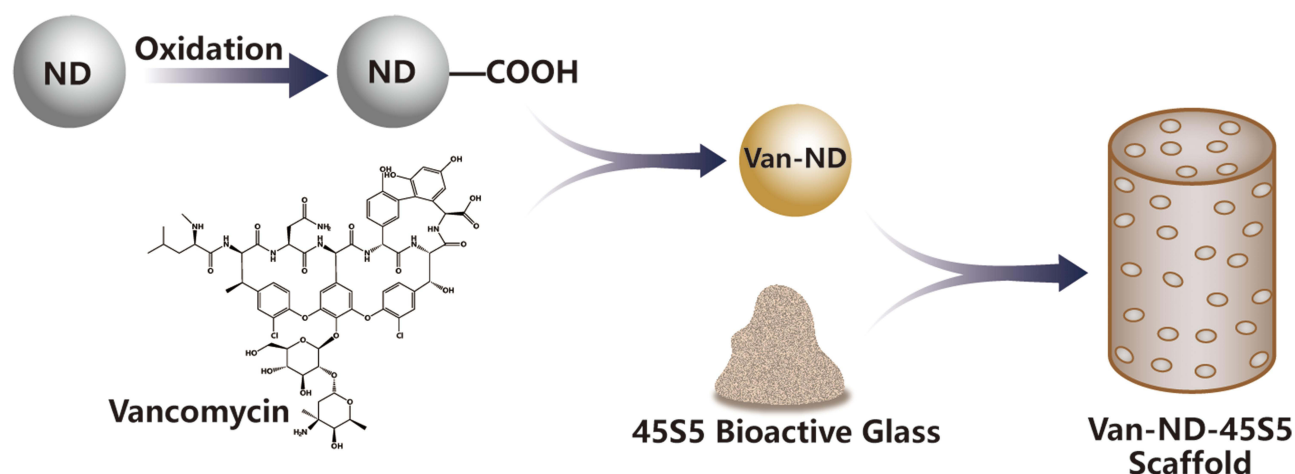


**Figure 1** The fabrication process of vancomycin-loaded ND and scaffold.

### Micromorphological Observation

Vancomycin-loaded ND and pure ND were dried in a vacuum drying oven, and their microstructures were observed under a SU-8100 scanning electronic microscope (Hitachi High-Tech, Tokyo, Japan).

### Mechanical Property

The compressive strength of all scaffolds (ND-45S5, Van-PLGA-45S5, and Van-ND-45S5 scaffolds) was measured using an RGD-5 Test Instruments (Shenzhen, Guangzhou, China).

### Porosity Determination

The porosity of all scaffolds (ND-45S5 scaffold, Van-PLGA-45S5 scaffold, and Van-ND-45S5 scaffold) was measured by micro-computed tomography (micro-CT) ( $\mu$ CT 80, Scanco Medical AG, Bassersdorf, Switzerland). Scaffolds were scanned at an energy of 3.0 kV, and the data were automatically evaluated using a CT analyzer. The region of interest (ROI) was monitored as a cube of dimensions 3 mm  $\times$  3 mm  $\times$  3 mm.

## Antibacterial Effect of the Scaffold in vitro

### Preparation of the Bacteria

*Staphylococcus aureus* is the most common pathogen associated with IBD.<sup>46</sup> In the present study, the *Staphylococcus aureus* ATCC25923 strain was obtained in freeze-dried form from ATCC and used to evaluate the antibacterial effect of the scaffolds.<sup>47</sup> The *Staphylococcus aureus* ATCC25923 strain was inoculated on the blood plate, followed by incubation at 37 °C for 24 h. Subsequently, several colonies were picked out and cultivated in MH (Mueller Hinton) broth, and their concentration was adjusted to 0.5 McFarland bacterial suspension by turbidimeter for standby.

### Bacterial Fluorescence Detection

Each group of scaffolds was placed in a 24-well plate containing the MH medium. The prepared *Staphylococcus* bacterial suspension was added to each well and incubated. Bacterial fluorescence in each group was detected at 6, 12, 18, and 24 h. The bacteria inoculated onto the scaffolds were fluorescently stained. The fluorescent dye SYSTO9 causes live bacteria to emit green fluorescence, and propidium iodide (PI) could make dead bacteria emit red fluorescence. The L7012 Invitrogen LIVE/DEAD BacLight Bacterial Viability Kit (Thermo Fisher Scientific, Waltham, MA USA) contained the two fluorescent dyes simultaneously. According to the manufacturer's instructions, the bacteria that adhered to the scaffold surface were stained with SYSTO9 and PI. The inoculated bacteria were observed using a confocal laser microscope.



### Antibacterial Circle Determination

Each scaffold group was placed in a culture dish containing MH broth. The prepared *Staphylococcus* bacterial suspension was added to an MH culture dish and incubated for bacterial culture. The diameter of the antibacterial circle in each group was measured on days 1, 2, 3, 4, 5, 6, 7, 8, 9, 10, and 11.

### Biocompatibility and Osteogenesis in vitro

Density gradient centrifugation combined with adherent culture was used to separate and culture rabbit bone marrow mesenchymal stem cells (BMSCs). First, the third and fifth generations of cells were inoculated onto the scaffolds for biocompatibility and osteogenesis in vitro. Briefly, BMSCs were cultivated in an osteogenic medium (DMEM/F12 supplemented with 10% heat-inactivated fetal bovine saline, ten mmol/L  $\beta$ -glycerophosphate, 50  $\mu$ mol/L ascorbic acid, and 0.1  $\mu$ mol/L dexamethasone) and then seeded in the blank control wells, ND-45S5, Van-PLGA-45S5 scaffolds, and Van-ND-45S5 scaffolds. Next, a McFarland *Staphylococcus aureus* suspension (0.5 mL) was added to the initial culture medium of each group. Subsequently, cells were maintained at 37 °C in a humidified atmosphere containing 5% CO<sub>2</sub>.

### Cell Morphology

The morphology of the cells was monitored after cell suspensions were seeded onto the scaffold surface ( $3 \times 10^5$  cells/scaffold). Following incubation for 7 d at 37 °C in a humidified atmosphere containing 5% CO<sub>2</sub>, the cell-seeded scaffolds were observed using scanning electron microscopy (SEM) (GeminiSEM 300, Carl Zeiss Meditec AG, Oberkochen, Germany).

### Cell Proliferation

The cytotoxicity and proliferation of cells were detected using a cell counting kit-8 (CCK-8) assay in vitro. Briefly, cells ( $4.5 \times 10^4/\text{cm}^2$ ) were seeded on blank control and scaffold-containing wells. Within 2 weeks of cell seeding, cells attached to the scaffold were washed with PBS and incubated in CCK-8 reagent every other day. The absorbance of each well was recorded using a microplate reader (Bio-Rad, Hercules, CA, USA) at a wavelength of 450 nm, and the proliferation curve of the inoculated cells in each group was plotted to evaluate the effect of various scaffolds on the cytotoxicity and proliferation of cells.

### Cell Cycle

The effects of the scaffolds on the cell cycle were assessed by flow cytometry. Briefly, cells ( $4 \times 10^4/\text{cm}^2$ ) were seeded on blank control and scaffold-containing wells. Seven days after seeding, the cells were collected, and cell cycle analysis was performed using a flow cytometer (FACS Calibur, BD, Franklin Lakes, NJ, USA).

### Cell Osteogenic Differentiation

The osteogenic differentiation of cells on different scaffolds in vitro was evaluated according to ALP activity. Briefly, cells ( $4 \times 10^4/\text{cm}^2$ ) were seeded into blank control and scaffold-containing wells. After 7 and 14 days of seeding, cells attached to the scaffold were rinsed with PBS, centrifuged, and then frozen in cell lysis buffer containing 0.2% Triton X-100 at -20 °C. The ALP enzyme concentration and total protein content were determined using an ALP assay kit (Abcam, London, UK) and a commercial total protein assay kit (Pierce, Rockford, IL, USA), respectively, following the manufacturer's instructions. ALP activity was defined as the ratio of the enzyme to protein concentration per scaffold.

### Cell Mineralization

The mineralization of cells on different scaffolds in vitro was evaluated using Alizarin Red S staining. Briefly, cells ( $4 \times 10^4/\text{cm}^2$ ) were seeded into blank control and scaffold-containing wells. After 7 days of seeding, the cells were washed, fixed, and stained using an Alizarin Red S staining kit (Genmed, Boston, MA, USA) following the manufacturer's instructions.

### Biocompatibility and Osteogenesis in vivo

#### Experimental Animal

The Experimental Animal Centre of the First Affiliated Hospital of Shandong First Medical University in Jinan, China, provided healthy adult New Zealand rabbits. The animal surgical protocols complied with the NIH guidelines for the care

and use of laboratory animals (NIH Publication No. 85–23 Rev. 1985), which were reviewed and approved by the Medical Ethics Committee of the First Affiliated Hospital of Shandong First Medical University (Approval No.2019S088).

### Establishment of an Animal Model of IBD

Sixty age- and weight-matched healthy adult New Zealand rabbits (3 months old) were used as experimental animals. All animals were housed in a single cage in the same breeding room with controlled temperature and humidity.

After the animals were successfully anesthetized with sodium pentobarbital, a lateral incision was made on the distal femur, and the lateral femoral condyle was separated and exposed. An orthopedic drill was used to create a bone defect with a diameter of 6 mm and depth of 6 mm on the lateral femoral condyle. Bone defects were sequentially washed with hydrogen peroxide and normal saline. After bleeding was stopped using sterile gauze,  $7 \times 10^6$  colony-forming units (CFU) of ATCC25923 *Staphylococcus aureus* were injected into the bone defect site, and the incision was closed by suture (Figure 2A).

After four weeks of administration, X-ray and puncture bacteriological examination methods were used to evaluate the modeling situation (Figure 2B and C), and experimental animals with successful modeling were selected for experiments in vivo.

### Implantation

Successfully modeled New Zealand rabbits were selected for in vivo evaluation. After anesthesia, the animals were randomly divided into four groups, with ten animals in each. The Sham-Op group was the sham-operation group, and the incision was sutured. In the group ND-45S5, no vancomycin-loaded ND-45S5 scaffolds were implanted into the infected defect site. In the group Van-PLGA-45S5, the Van-PLGA-45S5 scaffold was implanted into the infected defect site. Finally, in the group Van-ND-45S5, the Van-ND-45S5 scaffold was implanted into the infected defect site. After suturing, the animals were raised under the same conditions and observed daily.

### General Behavior of Animals

The mental state, dietary activities, and wound recovery of the animals were observed postoperatively.

### Radiographic Evaluation

At 6 and 12 weeks after the operation, five animals in each group were scanned by micro-CT, an area of the same size, including the implanted scaffold, was selected as the ROI, and changes in bone coverage (BC) and bone mineral density (BMD) between groups were analyzed.

### Histological Evaluation

At 6 and 12 weeks after the operation, after micro-CT scanning analysis, the specimens were trimmed and collected for hematoxylin and eosin (H&E) staining to observe the formation of new bone tissue and new bone trabecular structures. Images were obtained using the Olympus RX53 system (Olympus, Tokyo, Japan).

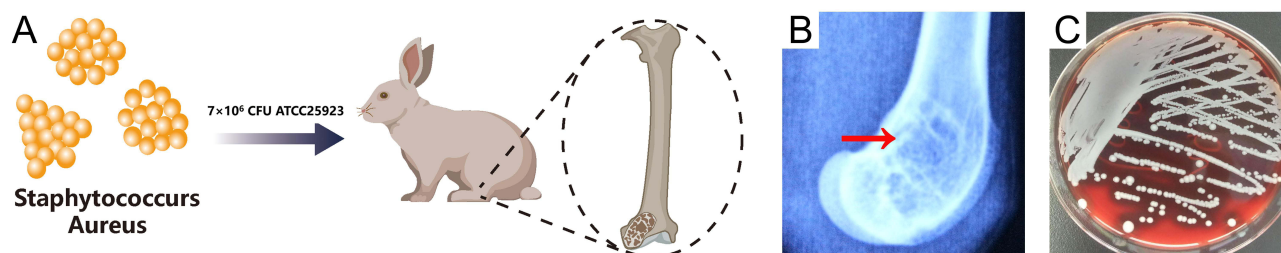


**Figure 2** Establishment of an animal model of IBD (A). A bone defect with a diameter of 6 mm and a depth of 6 mm on the lateral femoral condyle was created, and  $7 \times 10^6$  CFU of ATCC25923 *Staphylococcus aureus* was injected into the bone defect site. An animal model of IBD was validated using X-ray and puncture bacteriological examination methods after 4 weeks of administration. X-ray images showed the formation of a cavity in the femoral condyle with sequestrum (indicated by the arrow) (B); *Staphylococcus aureus* was found in a petri dish punctured for bacterial culture (C).

## Evaluation of the Bone Repair-Related Protein Expression

At 6 and 12 weeks after the operation, the specimens were trimmed after micro-CT scanning. The relative protein expression of VEGF, BMP, collagen I, and proteoglycan related to bone defect repair was detected by Western blot analysis.

## Statistical Analysis

Quantitative data are presented as mean  $\pm$  SD. Statistical analysis was assessed using SPSS (version 20, Chicago, IL, USA). A single factor analysis of variance (ANOVA) with Bonferroni's post hoc tests was performed to determine the statistical significance between experimental groups. Significance was considered at the level of  $p < 0.05$ .

## Results

### Characterization of Vancomycin-Loaded ND and Scaffold

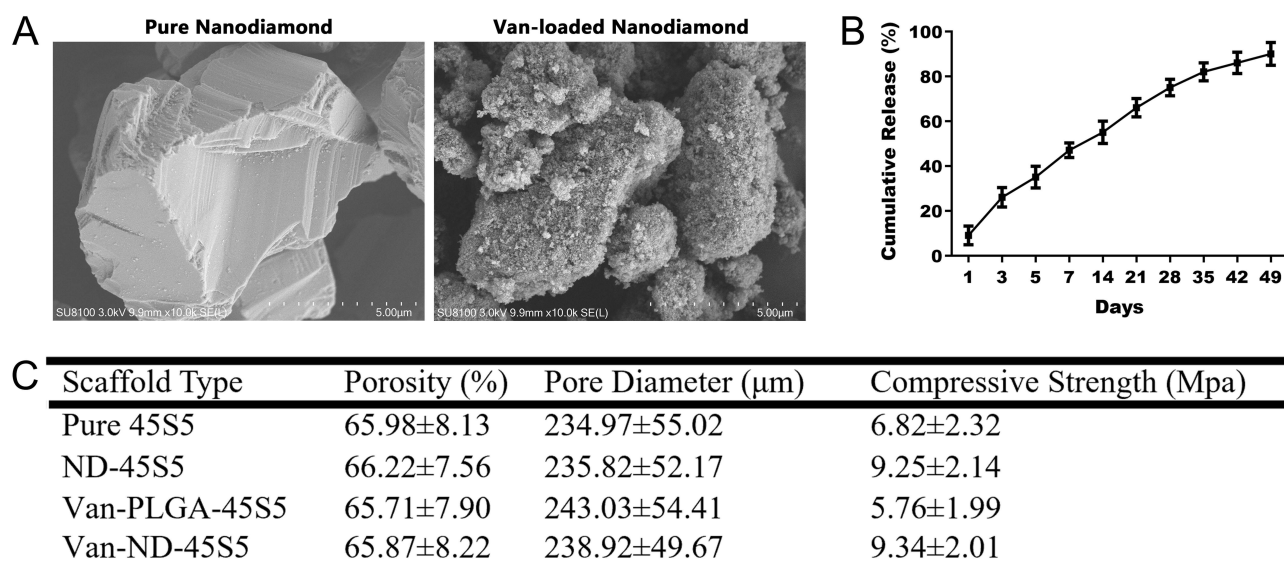
The pure ND ( $8.68 \pm 3.11 \mu\text{m}$ ) and vancomycin-loaded ND ( $8.90 \pm 3.52 \mu\text{m}$ ) were fabricated by an improved strong acid oxidation method. Figure 3A shows the microstructures of the pure ND and vancomycin-loaded ND. As a control, the encapsulation efficiency of vancomycin-loaded PLGA microspheres was approximately  $70.10 \pm 5.67\%$ . However, the encapsulation efficiency of vancomycin-loaded ND was approximately  $87.10 \pm 7.21\%$ , exhibiting high drug loading efficiency. Figure 3B indicates that vancomycin-loaded ND had a significant initial burst of vancomycin, of which  $>47\%$  was released within the first 7 days. The vancomycin release was nearly complete after 49 days.

Figure 3C presents the scaffolds' pore size, porosity, and compressive strength. The Van-ND-45S5 scaffold demonstrated a porosity of  $65.87 \pm 8.22\%$  and a pore diameter of  $238.92 \pm 49.67 \mu\text{m}$ . Overall, there were no significant pore size and porosity differences among the scaffolds. However, of note, the compressive strengths of the ND-45S5 scaffold and Van-ND-45S5 scaffold were  $9.25 \pm 2.14 \text{ MPa}$  and  $9.34 \pm 2.01 \text{ MPa}$ , respectively, which were higher than those of the pure 45S5 scaffold and Van-PLGA-45S5 scaffold ( $p < 0.05$ ).

## Antibacterial Effect of the Scaffold in vitro

### Bacterial Fluorescence Detection

Figure 4A shows that after co-cultivation of the *Staphylococcus aureus* ATCC25923 strain and scaffolds, there was no sustained release of antibiotics. ND-containing 45S5 scaffolds were filled with live bacteria showing green fluorescence, and dead bacteria showing red fluorescence were rarely found from 1–24 h of co-culture. With the extension of the co-



**Figure 3** SEM micrographs of the pure ND and Van-loaded ND morphology (A). The drug release profile of Van-loaded ND (B). Each value is mean  $\pm$  SD. Summary of structural and compressive strength of the Van-ND-45S5 scaffolds as compared with the control scaffolds (C).

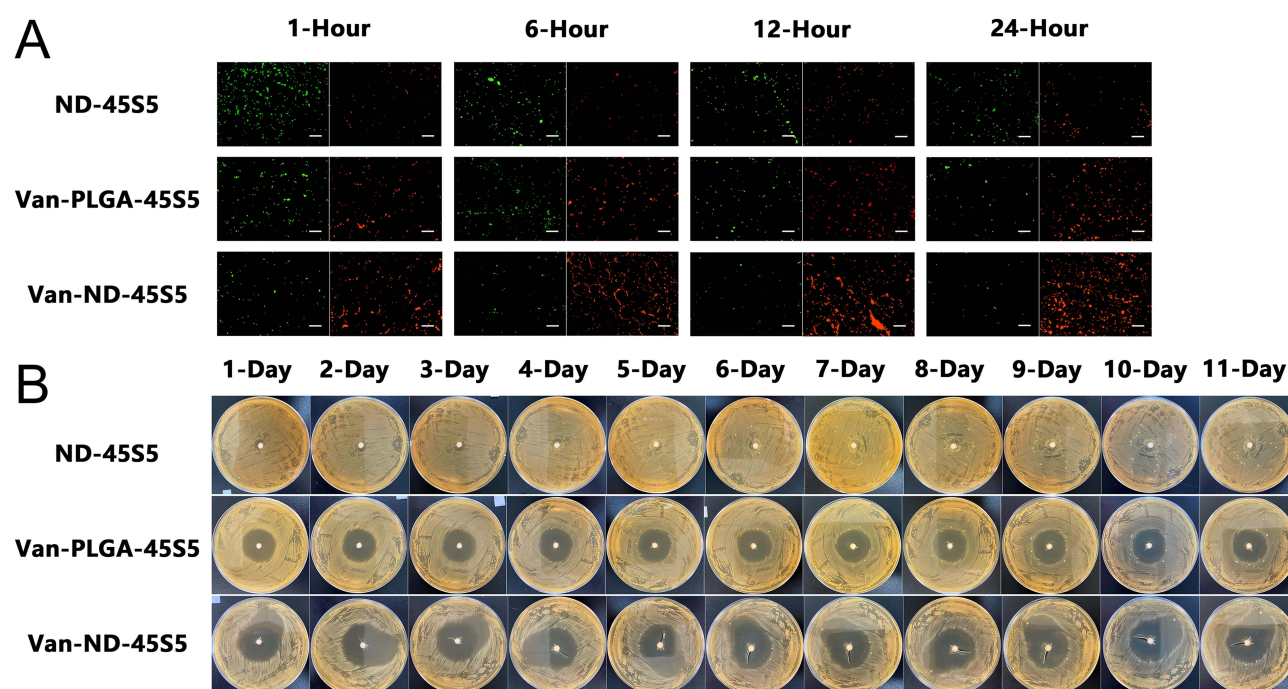


**Figure 4** Bacterial fluorescence detection at 1, 6, 18, and 24 h after co-culture of *Staphylococcus aureus* with scaffolds in each group (A). Scale bar = 150  $\mu$ m. Bacteria that emit green fluorescence were SYTO9-stained live bacteria, while bacteria that emit red fluorescence were PI-stained dead bacteria. Antibacterial circle determination at 1, 2, 3, 4, 5, 6, 7, 8, 9, 10, and 11 days after co-culture of *Staphylococcus aureus* with scaffolds in each group (B).

cultivation time, the number of viable bacteria in the ND-45S5 scaffolds gradually increased, while the number of dead bacteria gradually decreased. The Van-PLGA-45S5 and Van-ND-45S5 scaffolds were loaded with vancomycin, inhibiting bacterial growth and reproduction. However, due to the higher drug loading efficiency of the Van-ND-45S5 scaffold, from 1–24 h of co-cultivation, there were fewer live bacteria and more dead bacteria on the Van-ND-45S5 scaffolds than on the Van-PLGA-45S5 scaffolds as the co-cultivation time was prolonged.

### Antibacterial Circle Determination

After co-cultivation of the strains and scaffolds, ND-45S5 scaffolds without antibiotics were quickly surrounded by bacteria, and no bacteriostatic rings were found (Figure 4B). However, due to the slow release of vancomycin, antibacterial rings were revealed in both Van-PLGA-45S5 scaffolds and Van-ND-45S5 scaffolds, and from the 1st day to 11th day of co-culture, the diameters of the antibacterial rings of Van-ND-45S5 scaffolds ( $33.73 \pm 3.24$  mm) were significantly larger than those of Van-PLGA-45S5 scaffolds ( $26.45 \pm 2.53$  mm) (Figure 4B).

## Biocompatibility and Osteogenesis in vitro

### Cell Morphology

The morphology of the BMSCs on the scaffolds was observed using SEM. Figure 5A shows that the cells were attached and spread on both scaffold surfaces after 7 days of seeding. However, dense BMSCs were expanded and demonstrated on the Van-ND-45S5 scaffolds compared to the ND-45S5 scaffolds and Van-PLGA-45S5 scaffolds.

### Cell Proliferation

The CCK-8 assay was used to evaluate the cytotoxicity and proliferation of BMSCs on the various scaffolds. Figure 5B compares cell proliferation between the Van-unloaded and loaded scaffolds after 2, 4, 6, 8, 10, 12, and 14 days of seeding. With the extension of seeding, BMSCs in the blank control and ND-45S5 scaffolds without antibiotics gradually decreased in number. However, the OD value for Van-loaded scaffolds increased with increasing seeding time, revealing that the loaded vancomycin had an antibacterial effect, and the type of scaffold did not affect the viability and proliferation of BMSCs. Moreover, the OD value for the Van-ND-45S5 scaffolds was significantly higher than that of



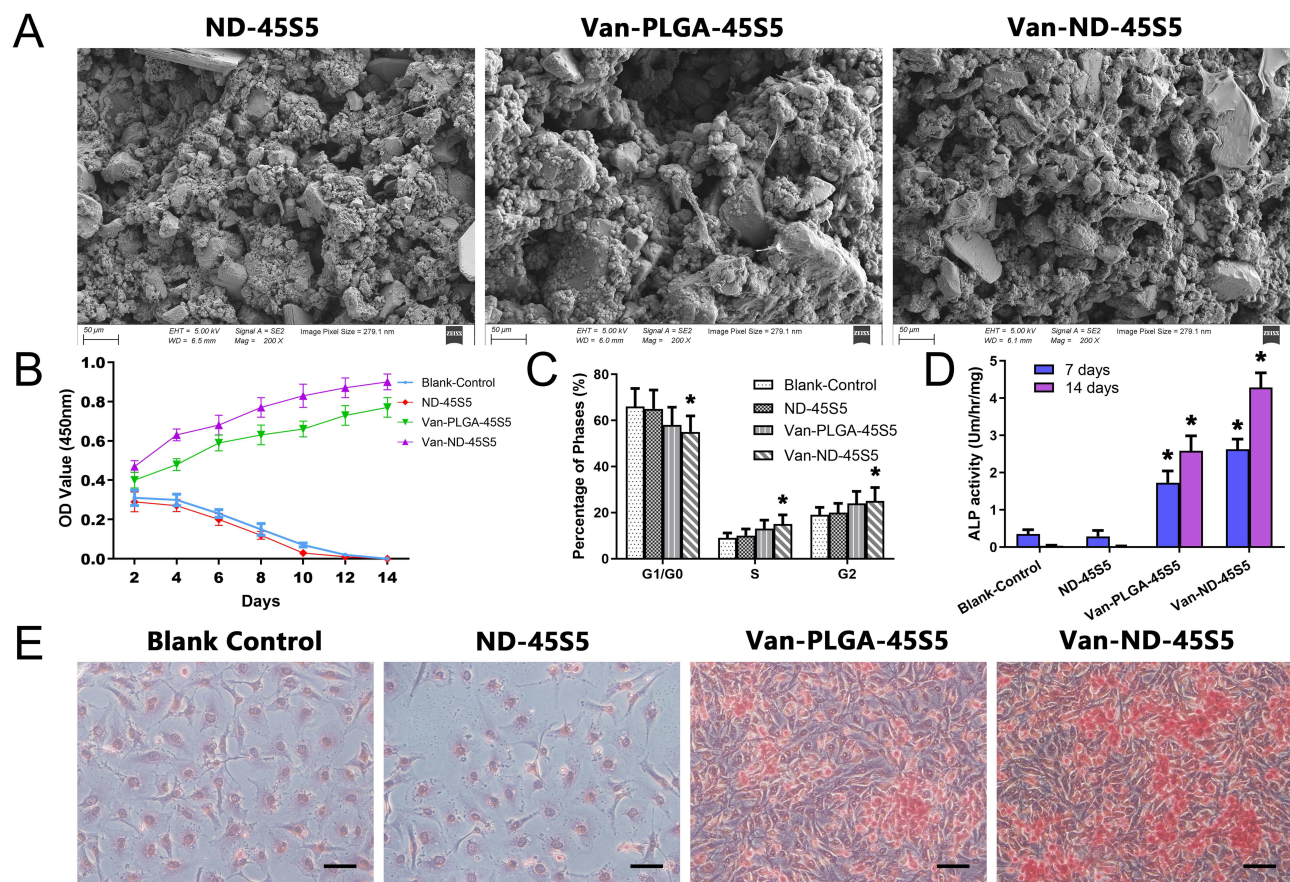


**Figure 5** SEM micrographs of cells on ND-45S5 scaffold, Van-PLGA-45S5 scaffold, and Van-ND-45S5 scaffold after 7 days of seeding (**A**). Cell proliferation of BMSCs was measured by CCK-8 assay within two weeks after cell seeding within each group (**B**). The percentage of BMSCs in each phase was measured by flow cytometry at 1 week after cell seeding within each group (**C**). ALP activity of BMSCs cultured on each group of scaffolds at 7 days and 14 days (**D**). Each value is mean  $\pm$  SD. \*  $p < 0.05$  was considered statistically significant according to the one-way ANOVA test followed by Bonferroni's post hoc tests. Cell mineralization of BMSCs was measured by Alizarin red S staining within 1 week after cell seeding within each group (**E**) (magnification: 400 $\times$ ). Scale bar = 150  $\mu$ m. The positively stained cells on the Van-ND-45S5 scaffold were significantly more than those on the blank controls, ND-45S5 scaffold, and Van-PLGA-45S5 scaffold.

the Van-PLGA-45S5 scaffolds after four days of seeding in the proliferation test ( $p < 0.05$ ), indicating its good anti-bacterial activity and biocompatibility. It was worth noting that two proliferation peaks were found in both groups of cells. Compared to the Van-PLGA-45S5 scaffolds (4–6 days, 10–12 days), the two proliferation peaks of BMSCs on the Van-ND-45S5 scaffolds (2–4 days, 6–8 days) appeared earlier.

### Cell Cycle

Flow cytometry was used to evaluate the cytotoxicity and cell cycle of BMSCs on the various scaffolds. **Figure 5C** shows that significantly more BMSCs in the S and G2 phases were found on the Van-ND-45S5 scaffolds than on the blank control and other scaffolds by day 7 ( $p < 0.05$ ). This finding also presented that the proliferation index of the Van-ND-45S5 scaffolds was significantly higher than that of the blank control and other scaffolds because of their excellent antibacterial activity and biocompatibility (**Figure 5C**).

### Cell Osteogenic Differentiation

Osteogenic differentiation was assessed by measuring the ALP activity of BMSCs cultured with different scaffolds. BMSCs cultured with Van-ND-45S5 scaffolds displayed significantly higher levels of ALP activity on days 7 and 14, followed by cells cultured with Van-PLGA-45S5 scaffolds (**Figure 5D**). Moreover, the ALP activity on the Van-ND-45S5 scaffolds significantly increased with the passage of cultivation time ( $p < 0.05$ ). However, no significant differences were observed in cells cultured with the blank control and ND-45S5 scaffolds, on days 7 and 14 after seeding, indicating low ALP activity (**Figure 5D**).

## Cell Mineralization

Figure 5E presents that the cell mineralization was assessed by Alizarin red S staining of BMSCs cultured with different scaffolds. After seeding for 7 days, the mineralization of BMSCs was highly expressed in cells cultured with the Van-ND-45S5 scaffolds (Figure 5E), suggesting that more BMSCs were differentiated into osteoblasts, followed by cells cultured with the Van-PLGA-45S5 scaffolds. No stained cells were observed in other groups.

## Biocompatibility and Osteogenesis in vivo

### General Behavior of Animals

All animals awoke 70 min post-implantation and were immediately weight-bearing. Wound infection was not observed in the Van-PLGA-45S5 and Van-ND-45S5 scaffold groups. Abnormal gait behavior was observed in most animals (18/20) after implantation in the Van-PLGA-45S5 and Van-ND-45S5 scaffold groups, whereas all animals recovered within 10 days without special treatment.

However, all animals in the control groups (sham-operation and ND-45S5 scaffold groups) presented with varying degrees of wound infection and abnormal gait behavior without special treatment.

### Radiographic Evaluation

High-resolution micro-CT imaging was performed to assess the formation of new bone trabeculae.

Figure 6A shows the 2D structure at 6 and 12 weeks post-implantation in each group, demonstrating the repair of bone defects in an infected microenvironment. We confirmed less new bone trabecular formation in the sham-operation group among the four groups, leaving the unrepaired defect at 6 and 12 weeks (Figure 6A). In the ND-45S5 scaffold group, only partially absorbed scaffolds and little new bone tissue appeared in the bone defect at 6 and 12 weeks (Figure 6A). Owing to the loaded antibiotics, the Van-PLGA-45S5 scaffold group revealed scattered new bone trabeculae in the infected defect site at 6 and 12 weeks (Figure 6A). However, in the infected defect site treated with the Van-ND-45S5 scaffold, the quality and morphology of new bone trabeculae were significantly improved compared with the other groups at 6 weeks. The IBD was almost completely healed at 12 weeks after implantation (Figure 6A).

Figure 6B and C shows the quantitative analysis of BC (Figure 6B) and BMD (Figure 6C) for each group. Averagely,  $7.89 \pm 3.34\%$  and  $12.14 \pm 4.00\%$  of each bone defect were repaired in the sham-operation group at 6 and 12 weeks, respectively. The ND-45S5 scaffold group demonstrated a BC of  $14.68 \pm 3.54\%$  and  $22.91 \pm 5.69\%$  at 6 weeks and 12 weeks, respectively. The Van-PLGA-45S5 scaffold group presented a BC of  $37.12 \pm 6.59\%$  and  $56.74 \pm 7.32\%$  at 6 and 12 weeks, respectively. In contrast, the BC was  $49.86 \pm 7.31\%$  (6 weeks) and  $75.15 \pm 9.32\%$  (12 weeks) in the Van-ND-45S5

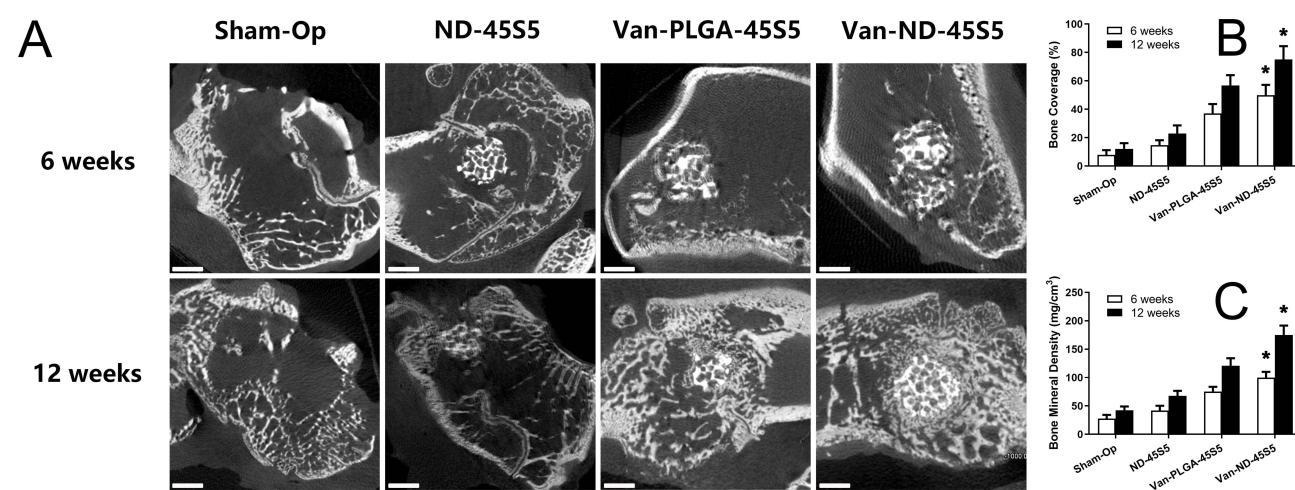


**Figure 6** Micro-CT scan analysis of 2D structure (A), BC (B), and BMD (C) of mineralized tissue formation after operation within each group. A statistically significant increase in new mineralized tissue appeared within the Van-ND-45S5 scaffold compared with control groups (sham-operation group, ND-45S5, and Van-PLGA-45S5 scaffold group) in IBD both after 6 and 12 weeks of operation. Scale bar = 3 mm. Each value is mean  $\pm$  SD. \*  $P < 0.05$  was considered statistically significant according to the one-way ANOVA test followed by Bonferroni's post hoc tests.



-45S5 scaffold group. BMD data revealed that Van-ND-45S5 scaffolds ( $99.86 \pm 10.31 \text{ mg/cm}^3$  at 6 weeks and  $175.15 \pm 16.32 \text{ mg/cm}^3$  at 12 weeks) resulted in more new bone trabeculae formed within the IBD compared with other groups. A statistically significant increase was confirmed in either BC or BMD between the Van-ND-45S5 scaffold group and other control groups (sham-operation group, ND-45S5 scaffold group, and Van-PLGA-45S5 scaffold group) ( $p < 0.05$ ).

### Histological Evaluation

Femoral condyle specimens from experimental animals were retrieved at 6 and 12 weeks postoperatively, and the formation of new bone tissue was assessed by histological analysis.

At 6 weeks after the operation, there was no evident formation of new trabeculae in the infected defects of the sham-operation group and the ND-45S5 scaffold group (Figure 7A). In the sham-operation and ND-45S5 scaffold groups, numerous inflammatory cells and fibrous tissue were found in the infected defect site or the porous scaffolds, whereas only a small amount of new bone tissue was observed in these two groups (Figure 7A). However, new bone trabeculae were observed in the Van-loaded scaffold-implanted infected defects (Figure 7A). Degradation of the gelatin microspheres and 45S5 BG matrices, as well as new bone formation, was observed at the outer edge of the scaffold. In the Van-PLGA-45S5 scaffold group, new bone trabeculae with inflammatory cells and fibrous connective tissue were observed inside the porous scaffolds (Figure 7A). In the Van-ND-45S5 scaffold group, the degradation of gelatin microspheres

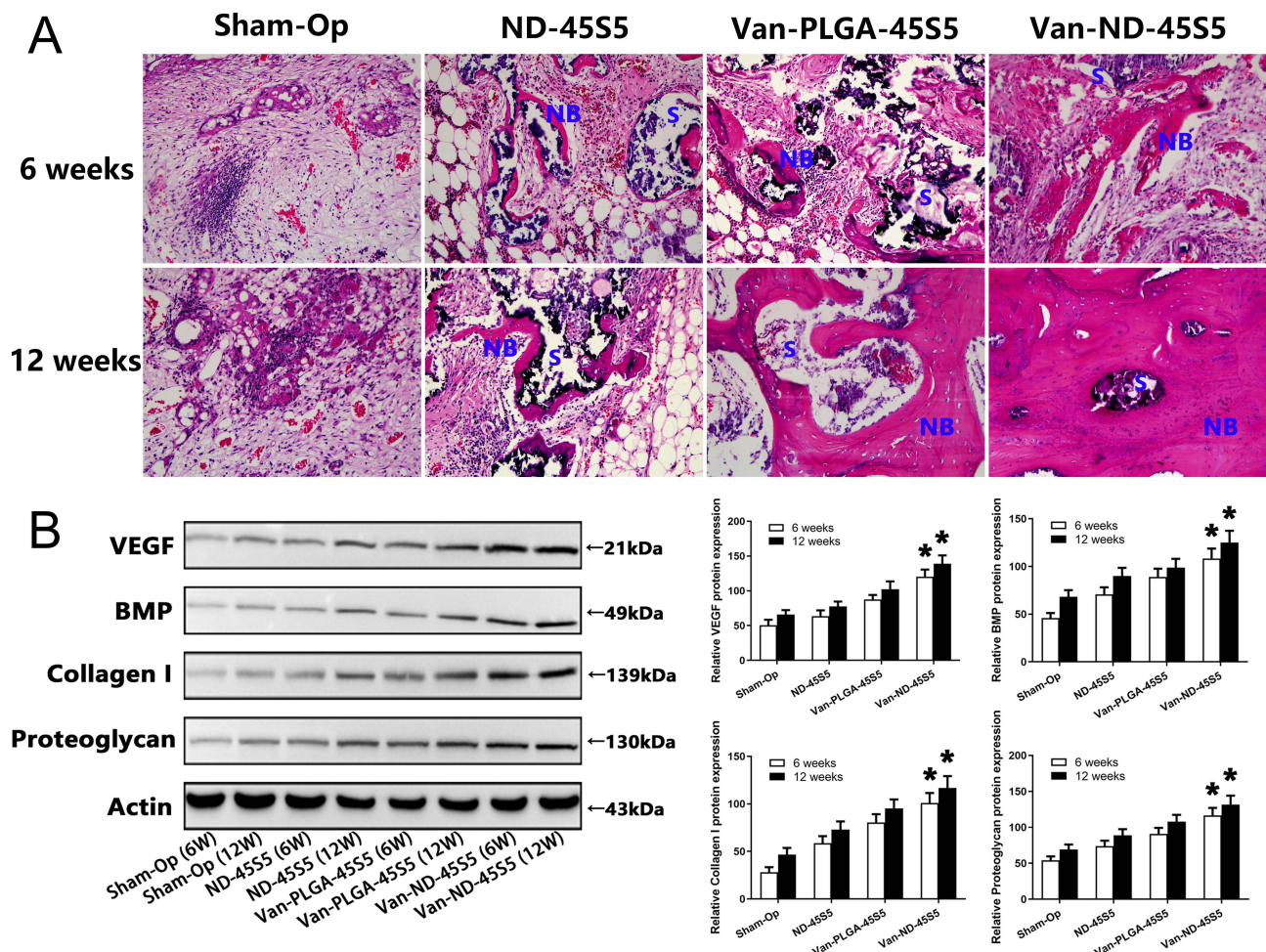


**Figure 7** Micrographs of H&E-stained sections (magnification: 200×) to observe new bone formation at 6 and 12 weeks after the operation or plus the implantation of ND-45S5 scaffold, Van-PLGA-45S5 scaffold, and Van-ND-45S5 scaffold (A). NB denotes the formation of new bone tissue and new bone trabecular structure, while S denotes scaffold materials. Western blotting images of the bone repair-related protein expression within each group after 6 and 12 weeks of operation (B). Compared with the sham-operation group, ND-45S5 scaffold group, and Van-PLGA-45S5 scaffold group, the relative expressions of VEGF, BMP, collagen I, and proteoglycan in the Van-ND-45S5 scaffold group were significantly increased both after 6 and 12 weeks of operation. Each value is mean  $\pm$  SD. \*  $p < 0.05$  was considered statistically significant according to the one-way ANOVA test followed by Bonferroni's post hoc tests.

resulted in porous cavities filled with some inflammatory cells, and more newly formed trabecular bone and fibrous tissue hyperplasia were detected between the trabecular bone (Figure 7A).

Twelve weeks after the operation, light microscopic images showed no sign of bone healing at the bone defect site in the sham-operated group (Figure 7A). Similarly, there was no integration between the scaffold and host bone in the ND-45S5 group (Figure 7A). Owing to the lack of sustained release of antibiotics, the inflammatory response at the bone defect sites in both groups was still severe (Figure 7A). In the Van-PLGA-45S5 scaffold group, mature bone trabeculae were formed with minimal inflammatory reactions (Figure 7A). With the prolongation of implantation time, the infected defect treated with the Van-ND-45S5 scaffold healed completely, and the new bone trabecular structure at the defect site was more mature and dense, while the inflammatory reaction disappeared (Figure 7A).

### Evaluation of the Bone Repair-Related Protein Expression

Western blot analysis was used to evaluate the expression of bone repair-related proteins, such as BMP, VEGF, collagen I, and proteoglycan. The expressions levels of BMP, VEGF, collagen I, and proteoglycan at 12 weeks in all groups were significantly higher than those at 6 weeks (Figure 7B) ( $p < 0.05$ ). Furthermore, the relative expressions of VEGF, BMP, collagen I, and proteoglycan in the Van-ND-45S5 scaffold group were significantly higher than those in the sham-operation group and other scaffolds both at weeks 6 and 12 after implantation (Figure 7B) ( $p < 0.05$ ).

## Discussion

As a type of bone defect challenging to heal, IBD is mainly caused by trauma, deformity, infection, and other factors, which have a high disability and deformity rate, prolonged healing time, and complex healing process, and occupy a lot of medical resources.<sup>48</sup> Moreover, its treatment requires both the healing of bone defects and the killing of infectious bacteria to maintain the sterile environment of the bone defect.<sup>49,50</sup> Therefore, IBD is a common issue faced by many disciplines, such as orthopedics clinics, medical materials science, and tissue engineering.<sup>51,52</sup>

Autologous bone transplantation is highly safe and considered the gold standard for bone defect repair, but the source of donors is limited.<sup>53,54</sup> However, rejection of allogeneic bone affects fracture healing.<sup>55</sup> An increasing number of scholars are currently focusing on the preparation of artificial bone repair materials<sup>56,57</sup> and local drug release systems.<sup>58,59</sup> Various composite bone scaffolds have achieved varying degrees of results in animal experiments.<sup>60,61</sup> Conventional antibiotic treatment is significantly compromised owing to the pathological structure of bone infections.<sup>62</sup> Local antibiotic treatment can achieve a high concentration of local antibiotics in the lesion, effectively killing and inhibiting the bacteria. Meanwhile, the deficiency of antibiotics in the peripheral blood dramatically reduces toxicity to internal organs and is safe to use.<sup>63</sup> Vancomycin has a deadly impact on common bacteria in IBD, such as *Staphylococcus aureus* and *Staphylococcus epidermidis*.<sup>64</sup> Although its sustained-release system has been used in research, the current drug-loading efficiency is not ideal.<sup>65,66</sup>

Guided by the treatment needs of clinical orthopedics, this study thoroughly used the knowledge integration of clinical medicine, medical materials, tissue engineering, and other disciplines to prepare composite tissue-engineered bone containing a high-efficiency vancomycin sustained-release system through bone tissue engineering technology and nanotechnology. Based to the literature and previous research, we used an improved acid oxidation method to functionalize the ND to prepare vancomycin-loaded ND with high drug loading efficiency and compared it with the existing vancomycin-loaded sustained-release system.<sup>41,67</sup> The evaluation indicated that ND had a higher drug loading efficiency than PLGA, with an encapsulation efficiency of 87%. Vancomycin-loaded ND was mixed with 45S5 BG with good biocompatibility, osteogenic activity, and degradability. The van-ND-45S5 scaffold could be prepared at room temperature to maximize the retention of vancomycin efficacy. In vitro evaluation revealed that vancomycin carried by the Van-ND-45S5 scaffolds could be continuously released for more than 49 days. By adding absorbable gelatin microspheres ( $240 \pm 32.25 \mu\text{m}$ ) during preparation, we obtained tissue-engineered bone with a suitable pore structure. According to our recent investigation,<sup>44</sup> 200–300  $\mu\text{m}$  is the most appropriate particle size for new bone ingrowth. In vitro results showed that all the scaffolds had good dispersion and were homogeneously distributed in the microspheres. The Van-ND-45S5 scaffold exhibited an average porosity of 65.87%, with a mean pore diameter of 238.92  $\mu\text{m}$ . The mechanical properties of the scaffold could be significantly improved by mixing ND with matrix materials, such as



45S5 BG. The 45S5 BG scaffold containing ND revealed that adding ND resulted in a higher compressive strength than the pure 45S5 BG scaffold. Moreover, carrying vancomycin did not affect the effect of ND on the mechanical properties of the scaffold. This finding is consistent with other scholars' findings.<sup>35,68</sup>

*Staphylococcus aureus* is a common pathogen in IBD.<sup>46</sup> In the present study, *Staphylococcus aureus* ATCC25923 was selected to evaluate the antibacterial effect of the scaffold in vitro.<sup>47</sup> With the extension of the co-cultivation time, bacterial fluorescence detection implied that the Van-ND-45S5 scaffold had reduced live bacteria and elevated dead bacteria compared with the other scaffolds. Meanwhile, the diameter of the antibacterial ring of the ND drug-loaded scaffold in the petri dish continued to maintain a diameter of  $33.73 \pm 3.24$  mm. In contrast, the non-drug-loaded scaffold group did not form antibacterial rings. The diameter of the antibacterial ring in the PLGA drug-loaded scaffold group was significantly smaller than that in the ND drug-loaded scaffold group. In vitro bacteriological studies confirmed that the Van-ND-45S5 scaffold had a satisfactory antibacterial effect relying on its efficient drug loading efficiency. Its sustained-release vancomycin continuously killed *Staphylococcus aureus* and maintained the antibacterial microenvironment around the scaffold, reflecting its continuous and effective anti-infective performance.

After the cells were inoculated into each group of scaffolds, SEM showed that the inoculated cells had good activity, reflecting the excellent biocompatibility of the Van-ND-45S5 scaffold. The cell proliferation curve and cell cycle analysis showed that the inoculated cells proliferated normally, the cell cycle was normal, and the Van-ND-45S5 scaffold had no biological toxicity. In vitro cytological studies verified that the Van-ND-45S5 scaffold exhibited good biocompatibility and osteogenic angiogenesis. Meanwhile, it had no apparent cytotoxicity and did not interfere with cell proliferation and the cell cycle. In the CCK8 assay, two proliferation peaks were observed for the BMSCs on Van-loaded scaffolds. We believe the first growth peak occurred because early cells were more vibrant. The second growth peak was attributed to the release of vancomycin from scaffolds, which killed bacteria and maintained a microenvironment more conducive to cell growth. ND exhibited more efficient drug loading efficiency. The Van-ND-45S5 scaffold completed its antibacterial activity earlier and maintained a sterile cell growth environment. Therefore, the two small peaks of the cell growth curve occurred earlier than those of the Van-PLGA-45S5 scaffold.

To evaluate the antibacterial effects of the scaffolds in vivo, we established an efficient animal model of IBD. We injected  $7 \times 10^6$  CFU of ATCC25923 *Staphylococcus aureus* into the bone defect of experimental animals according to previous studies.<sup>69</sup> This bacterial dose has a high local infection rate and does not easily cause systemic toxicity in animals. Therefore, it has the advantages of high modeling efficiency, low time consumption, and high economic cost. After four weeks of administration, imaging and puncture bacteriological examinations were performed to evaluate the modeling situation. We found that 90% of the experimental animals were successfully modeled. Experimental animals were selected for experiments in vivo. At 6 and 12 weeks after implantation of the scaffold, anesthetized animals were examined by puncture bacterial smear culture at the bone defect site, and micro-CT scanning was performed to analyze bone morphometric indices, such as BC and BMD of the local bone defect of the femoral condyle. Micro-CT results demonstrated that new bone trabeculae were observed around the Van-ND-45S5 scaffold when implanted into the infected defect site for 6 weeks. Twelve weeks after the operation, the Van-ND-45S5 scaffold formed a bone trabecula with a mature structure, closely connected with the surrounding bone without an obvious boundary. However, owing to the lack of local antibiotics, the bacteria quickly multiplied and proliferated after the non-drug-loaded scaffold was implanted into the IBD. The lesion's infection environment affected the bone defect's healing, and the ND-45S5 scaffold did not exert effective osteogenesis and angiogenesis. The healing of the bone defects at 6 and 12 weeks in this group was unsatisfactory. Owing to its relatively low drug loading efficiency, the Van-PLGA-45S5 scaffold had less osteogenic effect than the Van-ND-45S5 scaffold group in the infected environment. At 6 and 12 weeks postoperatively, the bone trabecular structure around the Van-PLGA-45S5 scaffold was weak and did not connect closely with the surrounding bone. Obvious boundaries were found between the new bone trabeculae and the Van-PLGA-45S5 scaffold. After radiographic evaluation, histological evaluation further verified the presence of many new bone trabeculae and angiogenesis in the specimens of the Van-ND-45S5 scaffold group. The expression of bone defect repair-related proteins at the mRNA and protein levels was relatively high in the Van-ND-45S5 scaffold group. Animal experiments have emphasized that the Van-ND-45S5 scaffold has an excellent antibacterial effect in vivo. Relying on highly loaded vancomycin, it

could continue to play an antibacterial role in IBD, provide an antibacterial environment, and continuously promote the healing of bone defects through its osteogenic activity.

## Conclusions

A Vancomycin-loaded ND-45S5 BG composite scaffold was prepared using bone tissue engineering technology and nanotechnology; and then systematically evaluated from the material, cytology, bacteriology, and zoology perspective. The results confirmed that its material properties could meet the treatment requirements for IBD and have good antibacterial effects and biocompatibility in vivo and in vitro. In addition, the Van-ND-45S5 scaffold could locally fill IBD, inhibit common IBD pathogens through slow-release vancomycin, give full play to its osteogenic activity, and significantly enhance the expression of VEGF, BMP, collagen I, and proteoglycan at the mRNA and protein levels, thus promoting the repair and healing of IBD and verifying its therapeutic effect in IBD.

This study revealed the therapeutic effect of the Van-ND-45S5 scaffold on IBD and expanded the research and application of bone tissue engineering and nanotechnology to bone infection-related diseases. The Van-ND-45S5 scaffold provide new materials and approaches for treating IBD; and has crucial scientific significance and clinical application value.

## Acknowledgments

The work was financially supported by the National Natural Science Foundation for Young Scientists of China (Grant No.81902188) and Cultivation Fund of the First Affiliated Hospital of Shandong First Medical University (Grant No. QYPY2019NSFC0804).

## Disclosure

We declare that none of the authors have any potential financial conflict of interest related to this manuscript.

## References

1. Azi ML, Teixeira AAA, Cotias RB, et al. Induced-membrane technique in the management of posttraumatic bone defects. *JBJS Essent Surg*. 2019;9(2):e22. doi:10.2106/JBJS.ST.18.00099
2. Luengo-Alonso G, Auñón Martín I, Rodríguez Vega V, et al. Long term results of lower limb posttraumatic acute bone defects treated with masquelet technique. *Injury*. 2021;52(Suppl 4):S99–S103.
3. Armstrong DG, Monahan K, Lehman EB, et al. The pediatric open supracondylar fracture: associated injuries and surgical management. *J Pediatr Orthop*. 2021;41(4):e342–e346.
4. Entezari V, Olson JJ, Vallier HA. Predictors of traumatic nerve injury and nerve recovery following humeral shaft fracture. *J Shoulder Elbow Surg*. 2021;30(12):2711–2719.
5. Dym H, Zeidan J. Microbiology of acute and chronic osteomyelitis and antibiotic treatment. *Dent Clin North Am*. 2017;61(2):271–282.
6. Mehra H, Gupta S, Gupta H, et al. Chronic suppurative osteomyelitis of mandible: a case report. *Craniofac Trauma Rec*. 2013;6(3):197–200.
7. Metsemakers WJ, Morgenstern M, McNally MA, et al. Fracture-related infection: a consensus on definition from an international expert group. *Injury*. 2018;49(3):505–510.
8. Debnar M, Kopp L, Misicko R. Management of bone defects using the Masquelet technique of induced membrane. *Rozhl Chir*. 2021;100(8):390–397.
9. Wong RMY, Li TK, Li J, et al. A systematic review on current osteosynthesis-associated infection animal fracture models. *J Orthop Translat*. 2020;23:8–20.
10. Wang W, Wang X, Wang Y, et al. Clinical study of autologous cartilage transplantation based on nano-hydroxyapatite in the treatment of talar osteochondral injury. *J Nanosci Nanotechnol*. 2021;21(2):1250–1258.
11. Laubach M, Suresh S, Herath B, et al. Clinical translation of a patient-specific scaffold-guided bone regeneration concept in four cases with large long bone defects. *J Orthop Translat*. 2022;34:73–84.
12. Zou Y, Huang B, Cao L, et al. Tailored mesoporous inorganic biomaterials: assembly, functionalization, and drug delivery engineering. *Adv Mater*. 2021;33(2):e2005215.
13. Xue X, Hu Y, Wang S, et al. Fabrication of physical and chemical crosslinked hydrogels for bone tissue engineering. *Bioact Mater*. 2021;12:327–339.
14. Folsch C, Sahm P, Ulloa CAF, et al. Effect of synthetic bone replacement material of different size on shear stress resistance within impacted native and thermoinfected cancellous bone: an in vitro femoral impaction bone grafting model. *Cell Tissue Bank*. 2021;22(4):651–664.
15. Nandi SK, Bandyopadhyay S, Das P, et al. Understanding osteomyelitis and its treatment through local drug delivery system. *Biotechnol Adv*. 2016;34(8):1305–1317.
16. Karki K, Sigdel S, Kaffle S. Is it worth adding systemic antibiotics to inhalational tobramycin therapy to treat pseudomonas infections in cystic fibrosis? *Cureus*. 2021;13(8):e17326.

17. Wang G, Luo W, Zhou Y, et al. Custom-made antibiotic cement-coated nail for the treatment of infected bone defect. *Biomed Res Int.* 2021;2021:6693906.
18. Qiu G, Huang M, Liu J, et al. Antibacterial calcium phosphate cement with human periodontal ligament stem cell-microbeads to enhance bone regeneration and combat infection. *J Tissue Eng Regen Med.* 2021;15(3):232–243.
19. Cui M, Pan H, Li L, et al. Exploration and preparation of patient-specific ciprofloxacin implants drug delivery system via 3d printing technologies. *J Pharm Sci.* 2021;110(11):3678–3689.
20. Olademehin OP, Kim SJ, Shuford KL. Molecular dynamics simulation of atomic interactions in the vancomycin binding site. *ACS Omega.* 2021;6(1):775–785.
21. Kizhakkekalam VK, Chakraborty K. Seaweed-associated heterotrophic bacteria: new paradigm of prospective anti-infective and anticancer agents. *Arch Microbiol.* 2021;203(3):1241–1250.
22. Ishaq H, Tariq W, Talha KM, et al. Association between high vancomycin minimum inhibitory concentration and clinical outcomes in patients with methicillin-resistant *Staphylococcus aureus* bacteremia: a meta-analysis. *Infection.* 2021;49(5):803–811.
23. Bruniera FR, Ferreira FM, Saviolli LR, et al. The use of vancomycin with its therapeutic and adverse effects: a review. *Eur Rev Med Pharmacol Sci.* 2015;19(4):694–700.
24. Zanjanzadeh Ezazi N, Shabbazi MA, Shatalin YV, et al. Conductive vancomycin-loaded mesoporous silica polypyrrole-based scaffolds for bone regeneration. *Int J Pharm.* 2018;536(1):241–250.
25. Jadidi A, Salahinejad E, Sharifi E, et al. Drug-delivery Ca-Mg silicate scaffolds encapsulated in PLGA. *Int J Pharm.* 2020;589:119855.
26. Almeida Neto GR, Barcelos MV, Ribeiro MEA, et al. Formulation and characterization of a novel PHBV nanocomposite for bone defect filling and infection treatment. *Mater Sci Eng C Mater Biol Appl.* 2019;104:110004.
27. Pacelli S, Acosta F, Chakravarti AR, et al. Nanodiamond-based injectable hydrogel for sustained growth factor release: preparation, characterization and in vitro analysis. *Acta Biomater.* 2017;58:479–491.
28. Cheng B, Pan H, Liu D, et al. Functionalization of nanodiamond with vitamin E TPGS to facilitate oral absorption of curcumin. *Int J Pharm.* 2018;540(1–2):162–170.
29. Torelli MD, Rickard AG, Backer MV, et al. Targeting fluorescent nanodiamonds to vascular endothelial growth factor receptors in tumor. *Bioconjug Chem.* 2019;30(3):604–613.
30. Jariwala DH, Patel D, Wairkar S. Surface functionalization of nanodiamonds for biomedical applications. *Mater Sci Eng C Mater Biol Appl.* 2020;113:110996.
31. Du X, Li L, Wei S, et al. A tumor-targeted, intracellular activatable and theranostic nanodiamond drug platform for strongly enhanced in vivo antitumor therapy. *J Mater Chem B.* 2020;8(8):1660–1671.
32. Gupta S, Evans B, Henson A, et al. Salt-assisted ultrasonicated de-aggregation and advanced redox electrochemistry of detonation nanodiamond. *Materials.* 2017;10:11.
33. Gao G, Guo Q, Zhi J. Nanodiamond-based theranostic platform for drug delivery and bioimaging. *Small.* 2019;15(48):e1902238.
34. Liu D, Qiao S, Cheng B, et al. Enhanced oral delivery of curcumin via vitamin E TPGS modified nanodiamonds: a comparative study on the efficacy of non-covalent and covalent conjugated strategies. *AAPS Pharm Sci Tech.* 2020;21(5):187.
35. Lim DG, Kang E, Jeong SH. pH-dependent nanodiamonds enhance the mechanical properties of 3D-printed hyaluronic acid nanocomposite hydrogels. *J Nanobiotechnology.* 2020;18(1):88.
36. Bondon N, Raehm L, Charnay C, et al. Nanodiamonds for bioapplications, recent developments. *J Mater Chem B.* 2020;8(48):10878–10896.
37. Dalai N, Sreekanth PSR. UHMWPE / nanodiamond nanocomposites for orthopaedic applications: a novel sandwich configuration based approach. *J Mech Behav Biomed Mater.* 2021;116:104327.
38. Westhauser F, Weis C, Prokscha M, et al. Three-dimensional polymer coated 45S5-type bioactive glass scaffolds seeded with human mesenchymal stem cells show bone formation in vivo. *J Mater Sci Mater Med.* 2016;27(7):119.
39. Wilkesmann S, Fellenberg J, Nawaz Q, et al. Primary osteoblasts, osteoblast precursor cells or osteoblast-like cell lines: which human cell types are (most) suitable for characterizing 45S5-bioactive glass? *J Biomed Mater Res A.* 2020;108(3):663–674.
40. Hoikkala NJ, Siekkinen M, Hupa L, et al. Behaviour of different bioactive glasses incorporated in polydimethylsiloxane endodontic sealer. *Dent Mater.* 2021;37(2):321–327.
41. Giammarco J, Mochalin VN, Haeckel J, et al. The adsorption of tetracycline and vancomycin onto nanodiamond with controlled release. *J Colloid Interface Sci.* 2016;468:253–261.
42. Jin S, Xia X, Huang J, et al. Recent advances in PLGA-based biomaterials for bone tissue regeneration. *Acta Biomater.* 2021;127:56–79.
43. Su Y, Zhang B, Sun R, et al. PLGA-based biodegradable microspheres in drug delivery: recent advances in research and application. *Drug Deliv.* 2021;28(1):1397–1418.
44. Zhang HX, Zhang XP, Xiao GY, et al. In vitro and in vivo evaluation of calcium phosphate composite scaffolds containing BMP-VEGF loaded PLGA microspheres for the treatment of avascular necrosis of the femoral head. *Mater Sci Eng C Mater Biol Appl.* 2016;60:298–307.
45. Li X, Xu J, Filion TM, et al. pHEMA-nHA encapsulation and delivery of vancomycin and rhBMP-2 enhances its role as a bone graft substitute. *Clin Orthop Relat Res.* 2013;471(8):2540–2547.
46. Gao J, Huang G, Liu G, et al. A biodegradable antibiotic-eluting PLGA nanofiber-loaded deproteinized bone for treatment of infected rabbit bone defects. *J Biomater Appl.* 2016;31(2):241–249.
47. Li Y, Liu YZ, Long T, et al. Mesoporous bioactive glass as a drug delivery system: fabrication, bactericidal properties and biocompatibility. *J Mater Sci Mater Med.* 2013;24(8):1951–1961.
48. Gage J, Liporace A, Egol A, et al. Management of bone defects in orthopedic trauma. *Bull Hosp Jt Dis.* 2018;76(1):4–8.
49. Corona PS, Altayo M, Amat C, et al. Reconstruction of infected post-traumatic bone defects of the distal femur with the compress® implant. Preliminary results of a staged non-biological strategy. *Injury.* 2021;52(3):606–615.
50. Xiao H, Wang S, Wang F, et al. Locking compression plate as an external fixator for the treatment of tibia infected bone defects. *Z Orthop Unfall.* 2021;2021:1.
51. Noaman HH. Management of upper limb bone defects using free vascularized osteoseptocutaneous fibular bone graft. *Ann Plast Surg.* 2013;71(5):503–509.

52. Wang M, Yang Y, Chi G, et al. A 3D printed Ga containing scaffold with both anti-infection and bone homeostasis-regulating properties for the treatment of infected bone defects. *J Mater Chem B*. 2021;9(23):4735–4745.
53. Klaue K, Knothe U, Anton C, et al. Bone regeneration in long-bone defects: tissue compartmentalisation? In vivo study on bone defects in sheep. *Injury*. 2009;40(Suppl 4):S95–S102.
54. Herath SC, Braun BJ, Rollmann MF, et al. Autologous transplantation of press-fit bone cylinders in the treatment of pelvic nonunion. *Orthop Surg*. 2019;11(3):516–523.
55. Ikehara S. Successful allogeneic bone marrow transplantation. Crucial roles of stromal cells in prevention of graft rejection. *Acta Haematol*. 2001;105(3):172–178.
56. Rustom LE, Poellmann MJ, Wagoner Johnson AJ. Mineralization in micropores of calcium phosphate scaffolds. *Acta Biomater*. 2019;83:435–455.
57. Li Z, Yang X, Liang S, et al. Imaging observation of nano-artificial bone in the repair of the defect in osteonecrosis of the femoral head. *J Nanosci Nanotechnol*. 2020;20(12):7775–7780.
58. Ding C, Li Z. A review of drug release mechanisms from nanocarrier systems. *Mater Sci Eng C Mater Biol Appl*. 2017;76:1440–1453.
59. Khatoon N, Chu MQ, Zhou CH. Nanoclay-based drug delivery systems and their therapeutic potentials. *J Mater Chem B*. 2020;8(33):7335–7351.
60. Dong Y, Liu W, Lei Y, et al. Effect of gelatin sponge with colloid silver on bone healing in infected cranial defects. *Mater Sci Eng C Mater Biol Appl*. 2017;70(Pt 1):371–377.
61. Wubneh A, Tsekoura EK, Ayranci C, et al. Current state of fabrication technologies and materials for bone tissue engineering. *Acta Biomater*. 2018;80:1–30.
62. Lew DP, Waldvogel FA. Osteomyelitis. *Lancet*. 2004;364(9431):369–379.
63. Zalavras CG, Patzakis MJ, Holtom P. Local antibiotic therapy in the treatment of open fractures and osteomyelitis. *Clin Orthop Relat Res*. 2004;2004(427):86–93.
64. Cheng T, Qu H, Zhang G, et al. Osteogenic and antibacterial properties of vancomycin-laden mesoporous bioglass/PLGA composite scaffolds for bone regeneration in infected bone defects. *Artif Cell Nanomed B*. 2018;46(8):1935–1947.
65. Wei S, Jian C, Xu F, et al. Vancomycin-impregnated electrospun polycaprolactone (PCL) membrane for the treatment of infected bone defects: an animal study. *J Biomater Appl*. 2018;32(9):1187–1196.
66. Zhang Y, Shen L, Wang P, et al. Treatment with vancomycin loaded calcium sulphate and autogenous bone in an improved rabbit model of bone infection. *J Vis Exp*. 2019;2019(145):e57294.
67. Mochalin VN, Neitzel I, Etzold BJ, et al. Covalent incorporation of aminated nanodiamond into an epoxy polymer network. *ACS Nano*. 2011;5(9):7494–7502.
68. Mangal U, Kim JY, Seo JY, et al. Novel Poly (Methyl Methacrylate) containing nanodiamond to improve the mechanical properties and fungal resistance. *Materials*. 2019;12:20.
69. Weng W, Li X, Nie W, et al. One-step preparation of an AgNP-nHA@RGO three-dimensional porous scaffold and its application in infected bone defect treatment. *Int J Nanomed*. 2020;15:5027–5042.

## International Journal of Nanomedicine

Dovepress

### Publish your work in this journal

The International Journal of Nanomedicine is an international, peer-reviewed journal focusing on the application of nanotechnology in diagnostics, therapeutics, and drug delivery systems throughout the biomedical field. This journal is indexed on PubMed Central, MedLine, CAS, SciSearch®, Current Contents®/Clinical Medicine, Journal Citation Reports/Science Edition, EMBase, Scopus and the Elsevier Bibliographic databases. The manuscript management system is completely online and includes a very quick and fair peer-review system, which is all easy to use. Visit <http://www.dovepress.com/testimonials.php> to read real quotes from published authors.

Submit your manuscript here: <https://www.dovepress.com/international-journal-of-nanomedicine-journal>